Quaternary International xxx (xxxx) xxx

Contents lists available at ScienceDirect

Quaternary International

journal homepage: www.elsevier.com/locate/quaint

Taxonomy, taphonomy and chronology of the Pleistocene faunal assemblage at Ngalau Gupin cave, Sumatra

Holly E. Smith [a,*], Gilbert J. Price [b], Mathieu Duval [c,a], Kira Westaway [d], Jahdi Zaim [e], Yan Rizal [e], Aswan [e], Mika Rizki Puspaningrum [e], Agus Trihascaryo [e], Mathew Stewart [f], Julien Louys [a]

[a] Australian Research Centre for Human Evolution, Environmental Futures Research Institute, Griffith University, Nathan, Queensland, 4111, Australia
[b] School of Earth and Environmental Sciences, The University of Queensland, St Lucia, Queensland, 4072, Australia
[c] Centro Nacional de Investigación Sobre la Evolución Humana (CENIEH), Burgos, 09002, Spain
[d] Department of Earth and Environmental Sciences, Macquarie University, Sydney, New South Wales, Australia
[e] Geology Study Program, Institut Teknologi Bandung, Jawa Barat, 40132, Indonesia
[f] Extreme Events Research Group, Max Planck Institutes for Chemical Ecology, the Science of Human History, and Biogeochemistry, Jena, Germany

ARTICLE INFO

Keywords:
Taxonomy
Taphonomy
Cave
Pleistocene
Southeast Asia
Hexaprotodon

ABSTRACT

Ngalau Gupin is a broad karstic cave system in the Padang Highlands of western Sumatra, Indonesia. Abundant fossils, consisting of mostly isolated teeth from small-to large-sized animals, were recovered from breccias cemented on the cave walls and unconsolidated sediments on the cave floor. Two loci on the walls and floors of Ngalau Gupin, named NG-A and NG-B respectively, are studied. We determine that NG-B most likely formed as a result of the erosion and redeposition of material from NG-A. The collection reveals a rich, diverse Pleistocene faunal assemblage (Proboscidea, Primates, Rodentia, Artiodactyla, Perissodactyla, Carnivora) largely analogous to extant fauna in the modern rainforests of Sumatra. The hippopotamid *Hexaprotodon* represents the only globally extinct taxon in deposits from Sumatra and the first record of this animal from the island. This deposit is dated using combined U-series/ESR dating analyses of several teeth that yield a finite age of between ~160 and ~115 ka, depending on the modalities of the dose rate evaluation. These ages constrain the fossil assemblage, not the breccia deposits. Since the direct U-series estimate obtained on the *Hexaprotodon* specimen is a minimum age, it is therefore not incompatible with the U-series/ESR results. Thus, the true age of the *Hexaprotodon* can possibly be between 160 and 115 ka, like the other fossil remains at Ngalau Gupin. These results suggest that the faunal assemblage at Ngalau Gupin correlates with late MIS 6 or early MIS 5. Ngalau Gupin likely reflects the formation of a fossil assemblage with two primary taphonomic pathways: a prime-aged dominated macrofauna component initially produced by carnivores but subsequently accumulated by porcupines and transported to the cave, and a microfauna component likely accumulated by small carnivores. Decalcification of the cemented deposit has further resulted in loss of fossil and other sedimentary material. This site adds important new chronologically constrained fossil mammal data for the Pleistocene record of Sumatra, an island relatively poorly investigated for Southeast Asia.

1. Introduction

The geological evolution and tropical climate of Southeast Asia created a global hotspot of biodiversity throughout the Pleistocene (Louys, 2008; Louys et al., 2007; Woodruff, 2010). Southeast Asia has a rich and interesting hominin history, highlighted by recent findings from Lida Ajer Cave, Sumatra, that demonstrate that *Homo sapiens* arrived in Southeast Asia before 63 ka - earlier than previously believed (Westaway et al., 2017); as well as other important hominin sites such as Trinil (Joorderns et al. 2009, 2015) and Ngandong, Java (Rizal et al., 2020) and Niah cave, Borneo (Barker et al., 2007). Many sites preserve a diverse suite of extant and extinct medium-to large-bodied mammals important for understanding the biogeographical and palaeoenvironmental history of the region (van den Bergh et al., 2001; Louys

* Corresponding author.
E-mail address: holly.smith11@griffithuni.edu.au (H.E. Smith).

https://doi.org/10.1016/j.quaint.2021.05.005
Received 28 May 2020; Received in revised form 5 May 2021; Accepted 6 May 2021
Available online 15 May 2021
1040-6182/

and Meijaard, 2010; Louys and Roberts, 2020). However, tropical caves are dynamic settings with complex formational processes, meaning it can be incredibly difficult to discern the taphonomic history of palaeontological and early human remains found within them (O'Connor et al., 2010; Morley and Goldberg, 2017; Smith et al., 2020). Studying mechanisms of site formation, depositional history, and faunal accumulation in Southeast Asian caves is therefore critical to our understanding of animal and hominin prehistory in Pleistocene Southeast Asia. Yet, compared to other regions such as tropical Africa, much less attention has been devoted to understanding the taphonomic and depositional histories of assemblages in tropical Southeast Asia.

During the last couple of decades, research has increasingly focussed on the faunal assemblages in the caves of Southeast Asia as a basis to resolve stratigraphic and depositional complexities (e.g. Bacon et al., 2004; Barker et al., 2007; Westaway et al., 2007; O'Connor et al., 2010; Mijares et al., 2010; Duringer et al., 2012; Bacon et al., 2015; Stephens et al., 2017; Morley et al., 2017; Louys et al., 2017; Westaway et al., 2017; Zeitoun et al., 2019). Nevertheless, few studies have been undertaken in the region of the Padang Highlands, the area with the earliest dated records of humans in the region (Westaway et al., 2017). Much of what we know about the Sumatran fossil record comes from palaeoanthropologist Eugene Dubois, (1891) and palaeontologist Dirk Albert Hooijer (Hooijer 1947a, 1947b, 1948, 1960, 1947b), who reported on and studied fossils from numerous caves, including Lida Ajer, Sibrambang, and Djamboe. Contextual information regarding these sites is largely missing, however, as many of the excavations were carried out prior to the development of modern excavation methods and, with the exception of Lida Ajer, because Dubois did not keep detailed field notes. The discovery in 2015 of a new fossil assemblage at Ngalau Gupin cave in the Padang Highlands (Louys et al., 2017) provides us with a unique opportunity to examine the taphonomic pathways fossils can take in a tropical cave setting. Here, we report on the taxonomy, taphonomy, and chronology of the vertebrate fossils from Ngalau Gupin.

2. Ngalau Gupin

Ngalau Gupin is a large limestone cave complex approximately 90 km east of Sawah Lunto City (00′ 38.685 S, 100' 38.823 E) (Fig. 1). This cave formed as part of a comprehensive karst system in Carboniferous-Permian limestones that includes several other previously reported caves (Dubois, 1891; Louys et al., 2017). Ngalau Gupin was first reported by Louys et al. (2017) as part of a survey of island Southeast Asian caves. Spot collection of isolated teeth from the Ngalau Gupin deposits was carried out, and initial U–Th dating of a *Tapirus* molar produced a preliminary minimum age of ~45 ka (Louys et al., 2017).

2.1. Site description

The site is easily accessed due to a relatively horizontal entrance and flat floor, walls and high ceiling. The entrance opens into a wide corridor that extends 15 m west and sits within the photic zone of the cave. The corridor opens almost immediately into a large cavernous chamber, averaging 12 m in width and 5 m in height. Abundant well-preserved Pleistocene fossiliferous breccia and sediments were identified in and around a phreatic U-shaped passage raised approximately 5 m from the lower cave floor (Fig. 2).

Breccia is present in two discrete areas in the U-shaped passageway. Non-fossiliferous breccia is visible on the eastern wall, evident as a 0.3 m deposit that hangs at most 2 m from the cave floor. The fossil-bearing breccia Ngalau Gupin-A (NG-A) is identifiable along the westernmost wall reaching a height of up to 1 m above the cave floor (Fig. 3). The breccia of NG-A represents a dense, lightly cemented mosaic deposit of angular clasts from pebble to cobble size within a clay-rich matrix. It is quite crumbly and appears significantly decalcified. Fossils were in general easily removed from this breccia by hand and pick.

Ngalau Gupin-B (NG-B) is demarcated as the unconsolidated fossil-bearing sediments visible on the topmost layer of the floor directly north of the U-shaped passageway (Fig. 4). NG-B has a surface area of approximately 5 × 5 m and a depth of ~10 cm, and visibly erodes to muddy topsoil that slopes approximately 2 m across the cave floor. The sediment deposits containing the NG-B assemblage are an unconsolidated clay-rich mud matrix.

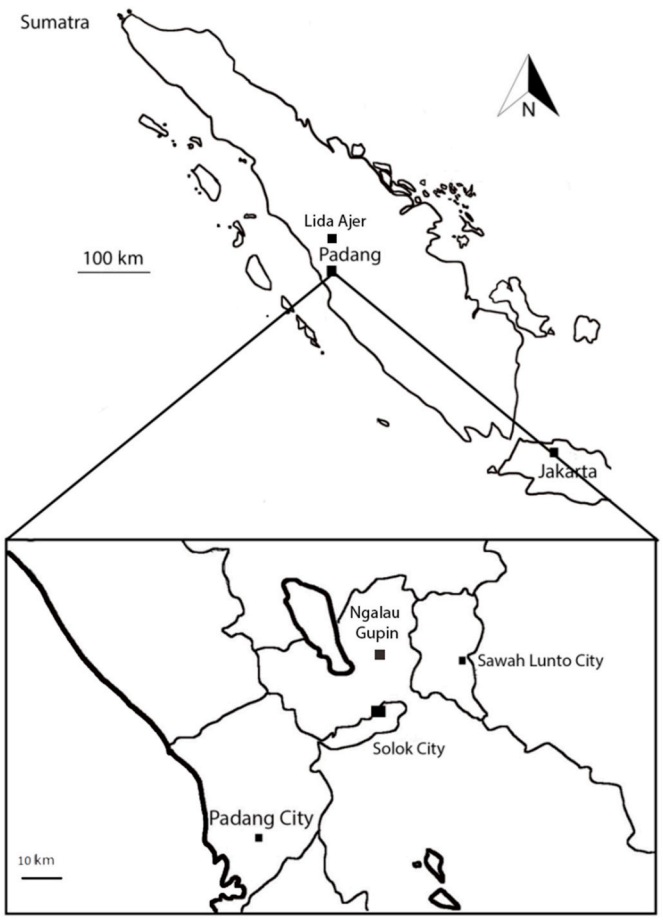

Fig. 1. Map of Sumatra illustrating the location of Padang (inset) and western Sumatra illustrating the location of Ngalau Gupin.

3. Methodology

3.1. Survey and excavation

In order to map the cave system, we performed a cave line survey, mapped by noting the orientation and inclination of the individual rooms and passages of Ngalau Gupin. These measurements were taken and recorded at regular intervals along a line transect and the two-dimensional data was used to form a scaled geometrical representation of the cave in lateral and plan view. Fossils visible in the breccia deposits were excavated using hammers and chisels. To remove adhering matrix, fossils were soaked in water for 24 h before mechanical preparation with a dental drill. The NG-B fossils in the unconsolidated sediments were excavated using trowels to a depth of 10 cm across a surface area of 3 × 1 m, with one protruding section in the west extending a further 1 × 0.5 m. The sediment was sieved through a 5 mm mesh and all faunal material was collected.

3.2. Systematic palaeontology

Every fossil specimen was identified to the lowest possible taxonomic level. The dimensions of the specimens were compared to osteological

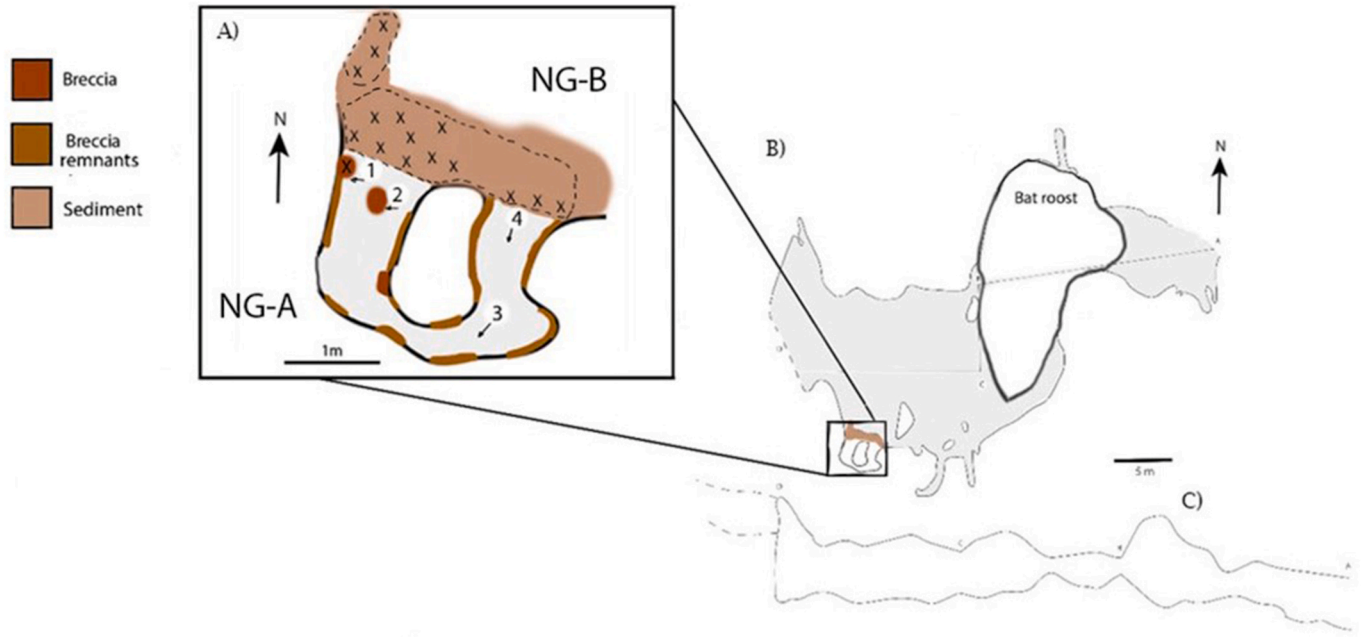

Fig. 2. Ngalau Gupin fossil site. A) Plan view of Ngalau Gupin breccia sites (inset); 1–4 are photograph locations and orientations presented in Fig. 3, the two areas indicated with the dashed lines are the sites of fossil excavation; the X indicates the presence of fossils in NG-B; B) plan view scale cave survey of Ngalau Gupin; C) lateral view scale cave survey of Ngalau Gupin.

collections housed at the Oxford Museum of Natural History, the Natural History Museum of London, Lee Kong Chian Natural History Museum, American Museum of Natural History and Zoologische Straatssammlung München. Classic measurements on teeth were taken to the nearest 0.1 mm. Dental nomenclature for each taxon was taken from well-established literature: Dental nomenclature for each taxon was taken from well-established literature: proboscideans (Maglio, 1927); felids (Hillson, 2005); viverrids (Popowics, 2003); *Helarctos* (Raffles, 1821 and Fitzgerald and Kraussman, 2002); primates (Kay, 1975; Teaford, 1982; Hooijer, 1948, 1960 and Drawhorn, 1995); *Hystrix* (Van Weers, 1990, 1993, 2005); rhinocerotids (Yan et al., 2014); suids (Cucchi, 2009); bovids (Hooijer, 1958; Suraprasit et al. 2016, 2020); cervids (Leslie, 2011; Chapman et al., 2005; Suraprasit et al., 2016); tragulids (Mennecart, 2018).

3.3. Taphonomic analysis

Taphonomic analysis was carried out following the established methods described below with each specimen examined by eye and hand lens (10x). Quantitative results are presented as Number of Identified Specimens (NISP) and the Minimum Number of Individuals (MNI) (Chaplin, 1971; Badgley, 1986; Lyman, 2008). MNI was calculated using the most abundant skeletal element or tooth and taking into consideration side (left/right) for bilaterally paired elements and age of the individual (Bunn et al., 1986). Elements were placed into an animal size class adapted from Bunn (1982); category I-II (<1 kg), category III-IV (1–10 kg), category V-VI (10–100 kg), category VII-VIII (100–340 kg) and category VIII-IX (>340 kg). Each specimen was assigned a weathering stage ranging from zero to five (following Behrensmeyer, 1978). Abrasion was recorded as: (1) little or no abrasion, retaining fresh, sharp edges; (2) moderate abrasion, exhibiting some rounding to breaks; and (3) heavy abrasion, with well rounded edges (following Shipman, 1977). Long bone fracture angle (oblique, right, oblique/right), outline (curved, transverse, intermediate), and edge (smooth, jagged) was recorded following Villa and Mahieu (1991). The animal age class was categorised by recording the wear stage of all whole teeth in the record in four categories: stage one, no apparent wear; stage two, little shear apparent and cusps blunted on most teeth; stage three, moderate shear apparent on facets and cusps; and stage four, strong shear facets and/or blunted cusps, premolars and molars very well-rounded. This categorisation was adapted from Brown and Chapman (1991) for Cervidae, Fitzgerald & Kraussman (2002) for Ursidae, Rolett and Chiu (1994) for Suidae, Hillson (2005) for Felidae, Tong et al. (2002) for Rhinocerotidae, Maffei (2003) for Tapiridae, Bowen and Coch (1970), Kay and Cant (1988), Bunn and Ungar (2009) for Cercopithecidae, Van Aarde (1985) for Hystricidae, and Sten (2004) for Bovidae. We used wear criteria given by crown height measurements in each of the relevant literatures to determine age classes for each taxon. Statistical analyses were carried out using PAST ver. 2.17c (Hammer et al., 2001). We list only representative specimens of each taxon evident in the collection (c. f. Leroy and Levinson, 1974; Hilton et al., 2001; Baludikay et al., 2016; Florin et al., 2020). The full taphonomic catalogue is available on an element-by-element database in the supplementary information (Table S10). The measurements in the database correspond to the anatomical tooth measurements described in section 3.2.

3.4. Abbreviations

Field numbers are denoted by the code SUMXX-xx, where XX refers to the year of collection and xx refers to the field number. From fieldwork undertaken in 2015, the NG-A specimens are identified with the abbreviation 'GUP1-51' and NG-B specimens are identified with abbreviation 'GUP52-81'. From fieldwork undertaken in 2018, the NG-A specimens are identified with the abbreviations 'GG', and NG-B specimens identified with the abbreviation 'NG'. Isolated specimens found within the cave but outside the NG-A and NG-B boundaries are denoted with 'GU'. All specimens are stored at Paleontologi dan Geologi Kuarter, Institut Teknologi Bandung, Indonesia.

3.5. Uranium profiling and combined U-series/ESR dating

3.5.1. Material

Six fossil teeth were collected from the cemented breccia and unconsolidated sediment deposits from Ngalau Gupin (Supplementary information Table S2) for uranium concentration profiling and/or direct dating, three from NG-A (SUM18-21, SUM18-26 & SUM18-27) and three

from NG-B (SUM18-22, SUM18-24 & GG4.1). Among these fossil teeth, five of them were dated using the combined U-series/ESR dating method, while the *Hexaprotodon* specimen GG4.1 was dated with U-series only. Corresponding sediment samples were collected at each locus (NG-A: SUM18-11; NG-B: SUM18-12) for dose rate reconstruction. The breccia matrix from NG-A was sampled for post infrared-infrared stimulated luminescence (pIR-IRSL) dating. This sample yielded very few potassium feldspar grains in the datable size range (90–212 μm) as seen in the Lida Ajer breccia (Westaway et al., 2017) and Ngalau Sampit (Duval et al. *in prep*). This amounted to only one single-grain disc of <100 grains, but none of these grains produced a measurable IRSL decay thereby preventing a reliable age estimation to be obtained.

3.5.2. Sample preparation

The five teeth were prepared following the standard ESR dating procedure based on enamel powder: the enamel layer was mechanically separated from the other dental tissues and both inner and outer surfaces were removed with a dentist drill to eliminate the volume that received an external alpha dose. The dentine attached to the enamel layer was kept aside for subsequent solution bulk U-series analyses. Enamel and

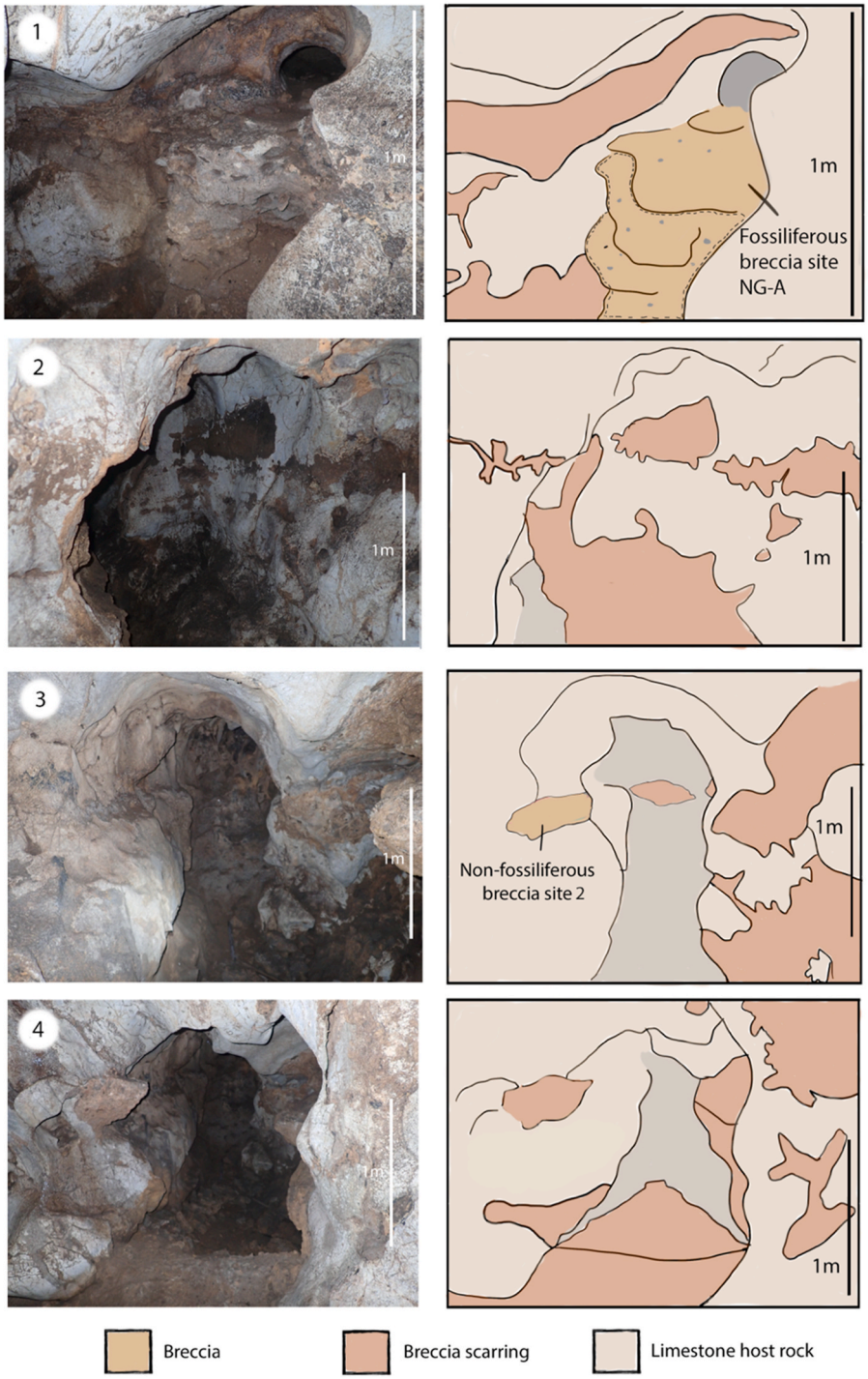

Fig. 3. Specific breccia remains observed in Ngalau Gupin at the excavation site of the NG-A assemblage. A-D) for locations and orientations of photographs refer to Fig. 2; (right) corresponding annotated sketches of photographs of breccia bearing site in Ngalau Gupin. The area within the dashed lines indicate the area that fossils were excavated from NG-A.

dentine were ground and sieved <200 μm. Unlike the other teeth dated, SUM18-21 was collected embedded in a breccia. The tooth was therefore extracted from the sediment, which was subsequently sampled for further analysis.

For uranium concentration profiling and U-series dating of sample GG4.1, powders were drilled across a transect from the enamel through the dentine using a 1 mm diameter stainless steel bit (see Price et al., 2013 for additional methodological details). GG4.1 was not further sampled for more destructive ESR dating considering its fragility and rarity as a representative specimen of *Hexaprotodon* in the deposit.

3.5.3. ESR dose evaluation

Dose evaluation used the multiple aliquot additive dose (MAAD) method. The enamel powder of sample SUM1821 was split into ten aliquots and gamma-irradiated at CENIEH (Spain) with a Gammacell 1000 Cs-137 gamma source (dose rate = 6.39 ± 0.15 Gy/min) to the following doses: 0.0, 49.9, 99.8, 149.6, 249.5, 349.2, 498.9, 698.5, 898.1 and 1496.8 Gy. The other enamel samples were irradiated at ANSTO (Australia) with a Co-60 source (dose rate = 13.23 ± 0.21 Gy/min) as follows: 0.0, 42.5, 83.3, 127.5, 206.8, 295.2, 427.7, 589.2, 769.0, 1283.0 and 2966.0 Gy.

Room temperature ESR measurements were carried out at CENIEH with an EMXmicro 6/1 Bruker ESR spectrometer coupled to a standard rectangular ER 4102ST cavity. The following procedure was used to minimise the analytical uncertainties: (i) all aliquots of a given sample were carefully weighted into their corresponding tubes and a variation of <1 mg was tolerated between aliquots; (ii) ESR measurements were performed using a Teflon sample tube holder inserted from the bottom of the cavity to ensure that the vertical position of the tubes remains exactly the same for all aliquots. The following acquisition parameters

Fig. 4. Fossiliferous sediments of NG-B and the entrance to the east and west passageways containing the NG-A remains excavated from consolidated breccia; (below) annotated sketch of the fossiliferous sediments containing the NG-B assemblage. The area within the dashed lines indicate the area in which the NG-B fossils were excavated.

were used: 1–50 scans, 1 mW microwave power, 1024 points resolution, 15 mT sweep width, 100 kHz modulation frequency, 0.1 mT modulation amplitude, 20 ms conversion time and 5 ms time constant. All aliquots of a given sample were measured within a short time interval (<1 h). This procedure was repeated two to three times over successive days without removing the enamel from the ESR tubes between measurements in order to evaluate measurement and equivalent dose (D_E) precisions (Supplementary Information Table S3).

The ESR intensities were extracted from T1-B2 peak-to-peak amplitudes of the ESR signal (Grün, 2000a), and then normalized to the corresponding number of scans and aliquot mass. D_E values were obtained by fitting a single saturating exponential (SSE) through the mean ESR intensities derived from the repeated measurements. Fitting was performed with Microcal OriginPro 9.1 software, which is based on a Levenberg-Marquardt algorithm by chi-square minimisation. Data were weighted by the inverse of the squared ESR intensity ($1/I^2$) (Grün and Brumby, 1994). ESR dose-response curves (DRCs) are shown in Supplementary Figure S1. Final 1-σ D_E error used for age calculation include both the fitting and gamma source dose rate errors.

3.5.4. Solution U-series analyses of dental tissues

Powdered enamel and dentine samples were weighed then spiked using a 229Th-^{233}U tracer before being digested in concentrated HNO_3. The solutions were then treated with H_2O_2 to remove trace organics, with U and Th then separated using conventional column chemistry techniques described in Clark et al. (2014). Both U and Th were collected into the same pre-cleaned test tube using 3 ml of 2% HNO_3 mixed with a trace amount of HF. U–Th isotopic ratios were then measured using a Nu Plasma multi-collector inductively-coupled plasma mass spectrometer (MC-ICP-MS) in the Radiogenic Isotope Facility at The University of Queensland, Brisbane, Australia, following analytical protocols described in Zhao et al. (2009), Price et al. (2013), and Clark et al. (2014).

3.5.5. Dose rate evaluation and age calculations

No *in situ* evaluation of the gamma dose rate associated with the teeth was performed. For all teeth except SUM18-21, both the beta and gamma dose rates were derived from the laboratory analysis of the corresponding bulk sediment samples collected at each locus. In contrast, for SUM18-21, two scenarios were considered, with beta and gamma dose rate derived from either the breccia sediment collected from around the tooth (a) or from sediment sample SUM18-11 collected at NG-A (b).

Inductively Coupled Plasma Mass Spectrometry (ICP-MS) analyses were performed on all sediment samples by Genalysis Laboratory Services, following a four-acid digest preparation procedure. The following parameters were used for the dose rate calculations: an alpha efficiency of 0.13 ± 0.02 (Grün and Katzenberger-Apel, 1994), Monte-Carlo beta attenuation factors from Marsh (1999), dose-rate conversion factors from Guérin et al. (2011), an assumed water content 5 ± 3 wt% in dentine. Current water (% wet weight) content in sediment samples SUM18-11 and SUM18-12 was evaluated to 24.9 and 26.6%, respectively. Consequently, a value of 25 ± 5% was assumed as long-term water content for all samples. Given the long distance between the cave entrance and the fossil teeth (>30 m), and the significant thickness of the overburden (ca. 30 m), the cosmic dose rate was assumed to be negligible. Post-Rn equilibrium was assumed in dental tissues and sediment.

DATA (Grün, 2009), a Quick Basic-based program was used to calculate US-ESR (based on the US model defined by Grün et al., 1988) and CSUS-ESR age estimates. The CSUS model defined by Grün (2000b) assumes a closed system behaviour after a rapid uranium uptake event in dental tissues. The CSUS-ESR age is usually considered as providing a maximum age constraint for the fossil. US and CSUS models are typically considered to encompass all possible uptake scenarios. Early uptake (EU)-ESR ages were also calculated for comparison. Finally, the accelerating uptake (AU) model (Shao et al., 2012) that can take into account uranium leaching was also tested. AU-ESR ages were obtained from USESR, a Matlab-based program (Shao et al., 2014). All combined U-series/ESR data inputs and outputs are given in Table 1.

4. Results

4.1. Taxonomic identifications

Class: Gastropoda Cuvier, 1795
Order: Stylommatophora Swainson, 1840
Representative specimen: GUP1 – mollusc – NG-A assemblage

(See Fig. 5, Fig. 5A)

GUP1 is a large mollusc. The spire, body whorl, and umbilicus of the shell are present, but the outer lip, palatal wall and columellar wall have been destroyed. The shell is depressed with five evident whorls; the apex of the shell has no growth lines and each whorl of the shell significantly increases in size from the interior to exterior. This sample has right-handed coiling. There are no identifiable ridges or plications to determine the genus of this specimen.

Order: Sigmurethra Bouchet & Rocroi, 2005
Family: Clausiliidae Gray, 1855
Representative Specimen: GUP27 – mollusc – NG-A assemblage

(Fig. 5B)

GUP27 is identifiable as a small brown Clausiliidae shell due to the oblong and elongate structure with five turreted whorls of equal size that coil sinistrally to a high spire (Loosjes, 1953; Dharma, 1992, 2005, 2005; Dharma et al., 2009). Shells are tapered at both ends and the aperture has a relatively oval shape and pronounced fold.

Class: Reptilia Laurenti, 1768
Order: Squamata Oppel, 1811
Family: Varanidae Merrem, 1820
Representative Specimens: NG4.1 – unidentified tooth – NG-B assemblage

(Fig. 5C)

This element is a sharp, pointed recurved tooth with a very lightly serrated edge. The tooth is laterally compressed and has two light ridges running down the lateral side of the tooth. This ridge is visible in the cross section of the tooth such that it is not perfectly circular. This dental morphology is typical of varanids (King and Green, 1999). There is a shallow depression in the tooth that extends across the enamel surface from either termination of the ridge. Overlapping morphology means that this tooth cannot be assigned to a species, however, varanids currently found in Sumatra include *Varanus dumerilii*, *Varanus rudicollis*, and *Varanus salvator*.

Class: Aves Linnaeus, 1758
Representative Specimens: NG34.17 – coracoid fragment - NG-B assemblage

(Fig. 5D)

NG34.17 is a coracoid with a transverse fracture along the shaft. The acrocoracoid process is present but poorly preserved. The general characteristics of the bone are typical of bird anatomy, such as the flaring out of the post coracoid process (Post, 2005; Kaiser, 2010), that is only partly preserved in this specimen. The lack of diagnostic material means that more specific identification is impossible.

Class: Mammalia Linnaeus, 1758
Order: Proboscidea Illiger, 1811
Family: Elephantidae Gray, 1821
Genus: *Elephas* Linnaeus, 1758
Elephas sp.

Table 1
Data inputs and outputs associated to the ESR age calculations. All errors are given at a 1σ confidence level. Key: (1) Apparent U-series ages are corrected for detrital Th. (2) A 10% error was assumed; (3) from sediment attached to SUM18-21; (4) from sediment sample SUM18-11 collected at NG-A; (5) from sediment sample SUM18-12 collected at NG-B; (6) corresponds to about 88% of the infinite-matrix gamma dose rate. In italics, AU-ESR age calculation outputs. SUM18-22a and SUM18-24a: age calculations using infinite matrix gamma dose rate; SUM18-22b and SUM18-24b: age calculations using 88% infinite matrix gamma dose rate.

SAMPLE	SUM18-21a	SUM18-21b	SUM18-22a	SUM18-22b	SUM18-24a	SUM18-24b	SUM18-26a	SUM18-26b	SUM18-27a	SUM18-27b
Locus	NG-A	NG-A	NG-B	NG-B	NG-B	NG-B	NG-A	NG-A	NG-A	NG-A
Enamel										
Dose (Gy)	35.1 ± 2.1	35.1 ± 2.1	32.8 ± 2.3	32.8 ± 2.3	33.6 ± 1.2	33.6 ± 1.2	26.1 ± 0.8	26.1 ± 0.8	22.2 ± 1.7	22.2 ± 1.7
U (ppm)	0.11 ± 0.00	0.11 ± 0.00	0.04 ± 0.00	0.04 ± 0.00	0.07 ± 0.00	0.07 ± 0.00	0.04 ± 0.00	0.04 ± 0.00	0.07 ± 0.00	0.07 ± 0.00
234U/238U	1.178 ± 0.004	1.178 ± 0.004	1.173 ± 0.003	1.173 ± 0.003	1.220 ± 0.006	1.220 ± 0.006	1.246 ± 0.003	1.246 ± 0.003	1.328 ± 0.006	1.328 ± 0.006
230Th/234U	0.390 ± 0.003	0.390 ± 0.003	1.438 ± 0.004	1.438 ± 0.004	0.582 ± 0.007	0.582 ± 0.007	0.397 ± 0.003	0.397 ± 0.003	0.430 ± 0.005	0.430 ± 0.005
230Th/232Th	34.8 ± 0.2	34.8 ± 0.2	38.7 ± 0.3	38.7 ± 0.3	64.8 ± 0.6	64.8 ± 0.6	34.7 ± 0.3	34.7 ± 0.3	79.9 ± 0.8	79.9 ± 0.8
Apparent U-series age (ka) (1)	52.1 ± 0.3	52.1 ± 0.3	60.8 ± 0.8	60.8 ± 0.8	91.1 ± 0.3	91.1 ± 0.3	53.2 ± 0.5	53.2 ± 0.5	59.3 ± 0.4	59.3 ± 0.4
Initial 234U/238U	1.209	1.209	1.208	1.208	1.287	1.287	1.289	1.289	1.390	1.390
Alpha Efficiency (1)	0.13 ± 0.02	0.13 ± 0.02	0.13 ± 0.02	0.13 ± 0.02	0.13 ± 0.02	0.13 ± 0.02	0.13 ± 0.02	0.13 ± 0.02	0.13 ± 0.02	0.13 ± 0.02
Water content (%)	0	0	0	0	0	0	0	0	0	0
Initial enamel thickness (μm) (2)	722 ± 72	722 ± 72	1803 ± 180	1803 ± 180	1474 ± 147	1474 ± 147	2467 ± 247	2467 ± 247	1593 ± 159	1593 ± 159
Dentine										
U (ppm)	5.28 ± 0.00	5.28 ± 0.00	4.47 ± 0.00	4.47 ± 0.00	3.37 ± 0.00	3.37 ± 0.00	4.66 ± 0.00	4.66 ± 0.00	3.70 ± 0.00	3.70 ± 0.00
234U/238U	1.148 ± 0.000	1.148 ± 0.000	1.062 ± 0.000	1.062 ± 0.000	1.052 ± 0.000	1.052 ± 0.000	1.097 ± 0.001	1.097 ± 0.001	1.091 ± 0.001	1.091 ± 0.001
230Th/234U	0.232 ± 0.001	0.232 ± 0.001	0.363 ± 0.001	0.363 ± 0.001	0.341 ± 0.001	0.341 ± 0.001	0.320 ± 0.001	0.320 ± 0.001	0.241 ± 0.000	0.241 ± 0.000
230Th/232Th	439.8 ± 1.7	439.8 ± 1.7	17950 ± 74	17950 ± 74	562.8 ± 1.7	562.8 ± 1.7	5972.0 ± 26.6	5972.0 ± 26.6	91.3 ± 0.2	91.3 ± 0.2
Apparent U-series age (ka) (1)	28.6 ± 0.1	28.6 ± 0.1	48.9 ± 0.1	48.9 ± 0.1	45.3 ± 0.1	45.3 ± 0.1	41.9 ± 0.0	41.9 ± 0.0	29.7 ± 0.1	29.7 ± 0.1
Initial 234U/238U	1.160	1.160	1.071	1.071	1.059	1.059	1.110	1.110	1.099	1.099
Water (%)	5 ± 3	5 ± 3	5 ± 3	5 ± 3	5 ± 3	5 ± 3	5 ± 3	5 ± 3	5 ± 3	5 ± 3
Removed enamel thickness (μm) (2)	7 ± 1	7 ± 1	239 ± 24	239 ± 24	115 ± 11	115 ± 11	212 ± 21	212 ± 21	211 ± 21	211 ± 21
Sediment										
U (ppm)	0.590 ± 0.072 (3)	3.720 ± 0.148 (4)	2.120 ± 0.101 (5)	2.120 ± 0.101 (5)	2.120 ± 0.101 (5)	2.120 ± 0.101 (5)	3.720 ± 0.148 (4)	0.590 ± 0.072 (3)	3.720 ± 0.148 (4)	0.590 ± 0.072 (3)
Th (ppm)	1.370 ± 0.075 (3)	3.040 ± 0.136 (4)	6.190 ± 0.263 (5)	6.190 ± 0.263 (5)	6.190 ± 0.263 (5)	6.190 ± 0.263 (5)	3.040 ± 0.136 (4)	1.370 ± 0.075 (3)	3.040 ± 0.136 (4)	1.370 ± 0.075 (3)
K (%)	0.441 ± 0.017 (3)	0.286 ± 0.011 (4)	0.434 ± 0.017 (5)	0.434 ± 0.017 (5)	0.434 ± 0.017 (5)	0.434 ± 0.017 (5)	0.286 ± 0.011 (4)	0.441 ± 0.017 (3)	0.286 ± 0.011 (4)	0.441 ± 0.017 (3)
Water (%)	25 ± 5	25 ± 5	25 ± 5	25 ± 5	25 ± 5	25 ± 5	25 ± 5	25 ± 5	25 ± 5	25 ± 5
Removed thickness (μm) (2)	34 ± 3	34 ± 3	15 ± 2	15 ± 2	110 ± 11	110 ± 11	77 ± 8	77 ± 8	18 ± 2	18 ± 2
US/AU-ESR age calculations										
internal dose rate (μGy/a)	11 ± 1	20 ± 4	*12 ± 12*	8 ± 1	*20 ± 1*	*19 ± 1*	*14 ± 1*	5 ± 1	*28 ± 1*	12 ± 2
beta dose rate, dentine (μGy/a)	23 ± 1	25 ± 2	*18 ± 18*	13 ± 2	*15 ± 1*	*13 ± 1*	*12 ± 1*	5 ± 0	*16 ± 1*	9 ± 1
beta dose rate, sediment (μGy/a)	54 ± 6 (3)	100 ± 11 (4)	*52 ± 4 (5)*	50 ± 6 (5)	*47 ± 4 (5)*	*46 ± 4 (5)*	*34 ± 4 (4)*	16 ± 2 (3)	*62 ± 6 (4)*	31 ± 4 (3)
Gamma + cosmic dose rate (μGy/a)	173 ± 14 (3)	460 ± 35 (4)	*465 ± 25 (5)*	409 ± 31 (5,6)	*465 ± 25 (5)*	*409 ± 31 (5,6)*	*460 ± 35 (4)*	173 ± 14 (3)	*460 ± 35 (4)*	173 ± 14 (3)
Total dose rate (μGy/a)	261 ± 15	606 ± 37	*547 ± 99*	481 ± 31	*547 ± 24*	*487 ± 31*	*520 ± 27*	200 ± 14	*555 ± 28*	225 ± 14
p enamel or *n enamel*	0.25	−0.93	*−0.025*	−0.92	*−0.027*	*−0.028*	*−0.030*	0.16	*−0.043*	−0.47
p dentine or *n dentine*	1.15	0.00	*−0.022*	−0.66	*−0.019*	*−0.015*	*−0.026*	.82	*−0.031*	−0.10
US-ESR age (ka) or *AU-ESR age (ka)*	**134 + 12–11**	**57 + 5–4**	***60 ± 10***	**68 + 7–6**	***61 ± 2***	***69 ± 3***	***50 ± 2***	**130 + 11–10**	***39 ± 3***	**98 + 10–9**
EU-ESR (ka)	**102 ± 7**	**53 ± 4**	**60 ± 5**	**67 ± 6**	**61 ± 4**	**68 ± 4**	**50 ± 3**	**119 ± 7**	**40 ± 4**	**90 ± 8**
CSUS-ESR (ka)	**141 ± 13**	**57 ± 5**	**60 ± 6**	**68 ± 7**	**60 ± 4**	**68 ± 5**	**50 ± 4**	**131 ± 10**	**39 ± 4**	**101 ± 10**

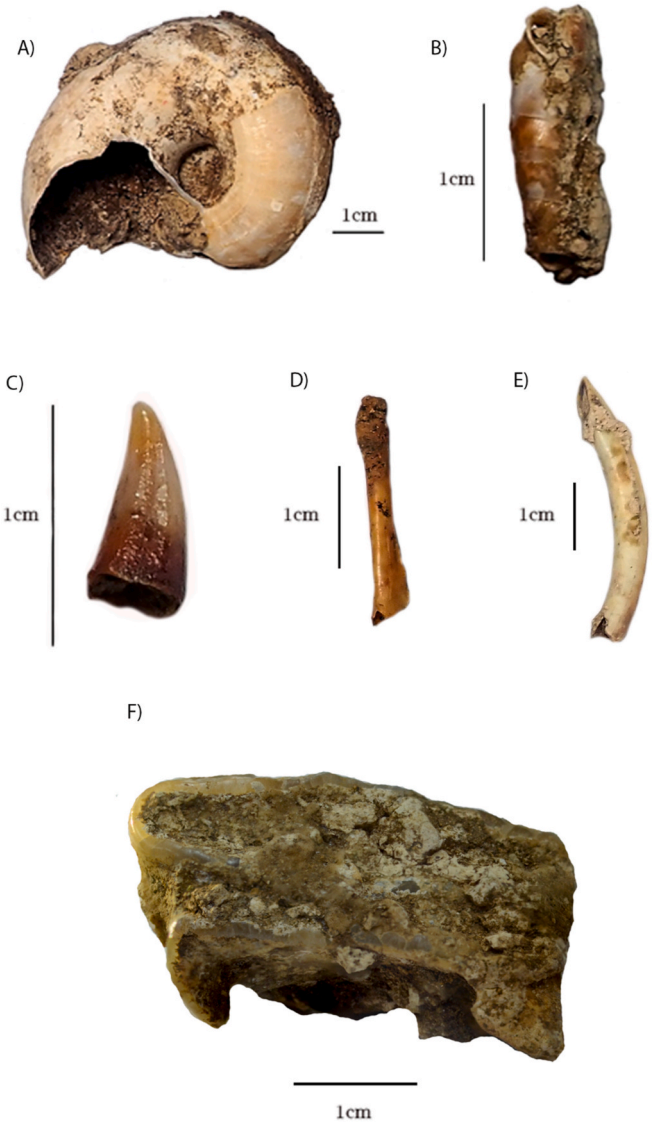

Fig. 5. (A) GUP1 Gastropoda shell in posterior view; (B) GUP27 Clausiliidae shell in posterior view; (C) NG4.1 Varanidae tooth; (D) NG34.17 Aves coracoid fragment; (E) NG3.38 *Hystrix* incisor in buccal view; (F) GUP52 *Elephas* sp. tooth plate fragment in occlusal view.

Representative specimen: GUP52 – molar fragment – NG-A assemblage

(Fig. 5F)

GUP52 is a molar fragment with typical hypsolophodont form. It preserves two elevated ridged enamel lamellae connected by depressed cementum. The enamel folds are heavily wrinkled and heavily worn. The widths of the lamellae (5.3 cm and 5.25 cm) are a strong indication that this fragment is an anterior section of a deciduous molar from a juvenile (Maglio, 1973). This specimen can be confidently assigned to Elephantidae as the two transverse cusp rows of the molar are fused into elevated loops of enamel with cementum infilling rather than roofed ridges (Zhang et al., 2017). It most likely belongs to *Elephas* sp.

Order: Primates, Linnaeus 1758
Family: Hominidae Gray, 1825
Genus: *Pongo* Lacépède, 1799
Pongo sp.

Representative Specimen: NG11.20 – left P^3 – NG-B assemblage

(See Fig. 6, Fig. 6A)

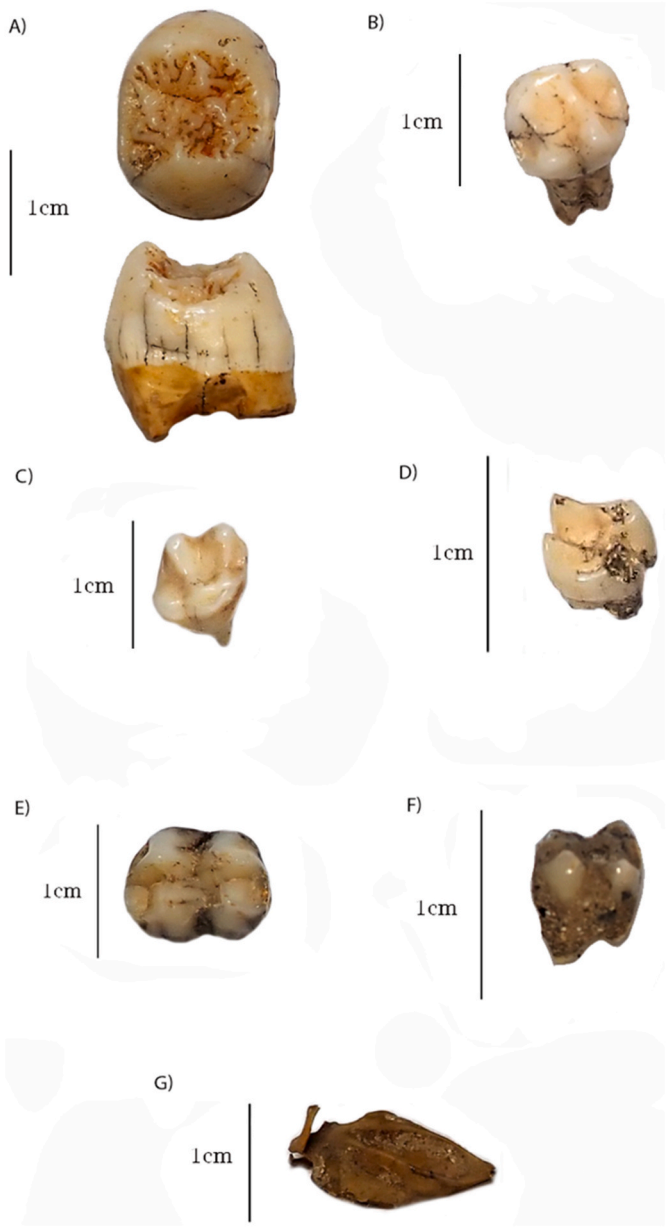

Fig. 6. (A) (above) NG11.20 *Pongo* sp., left P^3 occlusal view (below) and anterior view; (B) NG21.19 *Symphalangus*, left M^1; (C) *Hylobates*, right M^1; (D) NG13.14 *Presbytis*, right M^3; (E) GG1.10 *Nasalis*, left m_2; (F) NG20.10 *Macaca*, m_3; NG21.18 (G) NG34.14 Chiroptera, scapula.

The premolar is bunodont with numerous prominent crenulations extending between a large, pointed paracone, and a slightly smaller protocone. These are divided by a deep anteroposterior valley. Comparable morphology is seen in Pleistocene Southeast Asian specimens (Schwartz et al., 1994; Drawhorn, 1994; Bacon et al., 2001; Harrison et al., 2014; Filoux et al., 2015; Filoux and Wattanapituksakul, 2019). The tooth (15.11 mm in length and 12.26 mm in width) is larger than the average profile of modern *Pongo* specimens from Southeast Asia (Hooijer, 1948; Table S5), and towards the upper range of orangutan premolars recovered from other Pleistocene deposits in Sumatra (Hooijer, 1948). The taxonomy of fossil species is complicated for Sumatran *Pongo*, and so *Pongo* remains are not here assigned to species. Modern species that may be represented in the Ngalau Gupin collection include *Pongo abelii* (Lesson, 1827), and *Pongo tapanuliensis* (Nater et al., 2017).

Family: Hylobatidae Gray, 1870
Genus: *Symphalangus* Gloger, 1841
Species: *Symphalangus syndactylus* Raffles, 1821
Symphalangus syndactylus
Representative Specimen: NG21.19 – left M^1 – NG-B assemblage

(Fig. 6B)

NG21.19 is a first molar with four low, narrow reduced cusps. A prominent crista obliqua connects the protocone and metacone, with the ridge terminating lingually to the protocone. The paracone is wider than the protocone and the cusps are obliquely arranged, meaning that they form a rhombus, whereas in a lower second molar the anterior cusps would more-or-less form a square. The teeth excavated from this sample are too large to be considered *Hylobates agilis*; the gibbon found at Lida Ajer cave in the Padang Highlands (Hooijer, 1948, 1960). The dimensions of this sample fit well within the range of *Symphalangus syndactylus* from Southeast Asia (Hooijer, 1960; Frisch, 1967; supplementary Table S5).

Genus: *Hylobates* Illiger, 1811
Hylobates sp.
Representative Specimen: NG21.18 – right M^1 – NG-B assemblage

(Fig. 6C)

NG21.18 is an enlarged, broad crown that is marginally compressed laterally. This tooth is distinguished as a *Hylobates* molar due to the characteristic hypocone as the highest cusp, with the tooth wider than it is long (Hooijer, 1960). The dimensions of the tooth are within the range of the *Hylobates* from Southeast Asia (Hooijer, 1960; Frisch, 1967; supplementary Table S5).

Family: Cercopithecidae Gray, 1821
Subfamily: Colobinae Jerdon, 1867
Genus: *Presbytis* Eschscholtz, 1821
Presbytis sp.

Representative specimen: NG13.14 –right M^3 – NG-B assemblage
(
Fig. 6D)

The overall morphology is typical of cercopithecine third molars, but this tooth has a critical characteristic that differs significantly in Presbytis from all other Asian colobines; the distal cusps are joined with no separation between crests (Willis and Swindler, 2004). The size range (6.1 mm in length and 5.29 mm in width) overlaps with the average profile for *Presbytis* molars (Swindler, 2002).

Genus: *Nasalis* St Hilaire 1812
Nasalis sp.
Representative Specimen: GG1.10 – left m_2 – NG-A assemblage

(Fig. 6E)

GG1.10 can be categorised as a left lower second molar of *Nasalis* due to the greater integration of the transverse lophs and less pronounced trigonid in comparison to other Old World Monkeys (Swindler and Orlosky, 1974). The tooth is stout and rounded with a bilophodont structure, and four highly pointed cusps that rapidly decline into a deep valley across the occlusal surface. The most pronounced cusp is the hypoconid, followed by the protoconid, the paraconid and finally the stout metaconid.

Subfamily: Cercopithicinae Gray, 1821
Genus: *Macaca* Lacépéde, 1799
Macaca sp.
Representative Specimen: NG20.10 – m_3 – NG-B assemblage

(Fig. 6F)

The third molar crown of NG20.10 is bilophodont with four sharp high cusps with a prominent distoconulus. There is a narrow groove running from the base of the cusps to the terminus of the enamel on the lingual and buccal surfaces of the molar. This specimen is identifiable as a *Macaca* molar due to the significant lingual groove; deeply defined to half of the width of the tooth, terminating at a perpendicular intersection with a small enamel ridge outlining the central tooth basin (Kay, 1978; Teaford, 1982). The four cusps of the molar are more prominent than those of the more derived molars of *Pongo*. Unlike the oblique arrangement of the *Symphalangus* molars, the cusps form a large square in occlusal view.

Order: Rodentia Bowdich, 1821
Family: Hystricidae Fischer de Waldheim, 1817
Genus: *Hystrix* Linnaeus, 1758
Hystrix sp.
Representative Specimen: NG3.38 – lower incisor – NG-B assemblage

(Fig. 5E)

The characteristic chisel-like shape and triangular cross-section with a slightly convex shape of NG3.38 are consistent with *Hystrix* lower incisors (e.g. Van Weers, 2005). The striking similarities in morphology between species (Van Weers, 2005; Monchot et al., 2012) and the overlap of the Ngalau Gupin specimens with the dimensions of the modern and extinct species from museum collections preclude specific diagnoses at this stage.

Order: Chiroptera Blumenbach, 1779
Representative Specimen: NG34.14 – right scapula – NG-B assemblage

The bone specimen NG34.14 is a right scapula. The scapula of Chiroptera have a distinctive morphology, including a reduced acromion process, a single articular surface and a globular glenoid cavity (Schlosser-Sturm and Schliemann, 1995; Panyutina et al., 2013).

Order: Artiodactyla Owen 1848
Family: Suidae Gray, 1821
Genus: *Sus* Linnaeus, 1758
Sus scrofa Linnaeus, 1758
Representative Specimen: NG30.10 – right M^3 – NG-B assemblage

(See Fig. 7, Fig. 7A)

The molar NG30.10 has very typical features of a suid: tall rounded bunodont cusps and numerous enamel projections creating an irregular occlusal surface (Cucchi et al., 2009; Berkovitz and Shellis, 2018). This molar is assigned to *Sus scrofa* on the basis of its relatively short and wide shape, with no obvious heptaconule. See supplementary Table S6 for the dimensions of suid teeth in the Ngalau Gupin collection.

Sus barbatus Müller, 1838
Representative Specimen: NG30.12 – right M^3 – NG-B assemblage

(Fig. 7B)

The molar is morphologically similar to that of *Sus scrofa* but is distinguished by the rugose enamel on the molar and the presence of bulky accessory tubercles most consistent with those of *Sus barbatus*, whereas tubercles in other suids are typically lacking (Tougard, 1998). This tooth falls within the size range of teeth taxonomically assigned to *Sus cristata* and *Sus barbatus* from Duoi U'Oi, Vietnam (Bacon et al., 2008; See supplementary Table S6). The considerable overlap in size makes identification difficult.

Family: Hippopotamidae Gray, 1821
Genus: *Hexaprotodon* Falconer and Cautley, 1836
Hexaprotodon sp.
Representative Specimen: GG4.1 – left m_2 – NG-A assemblage

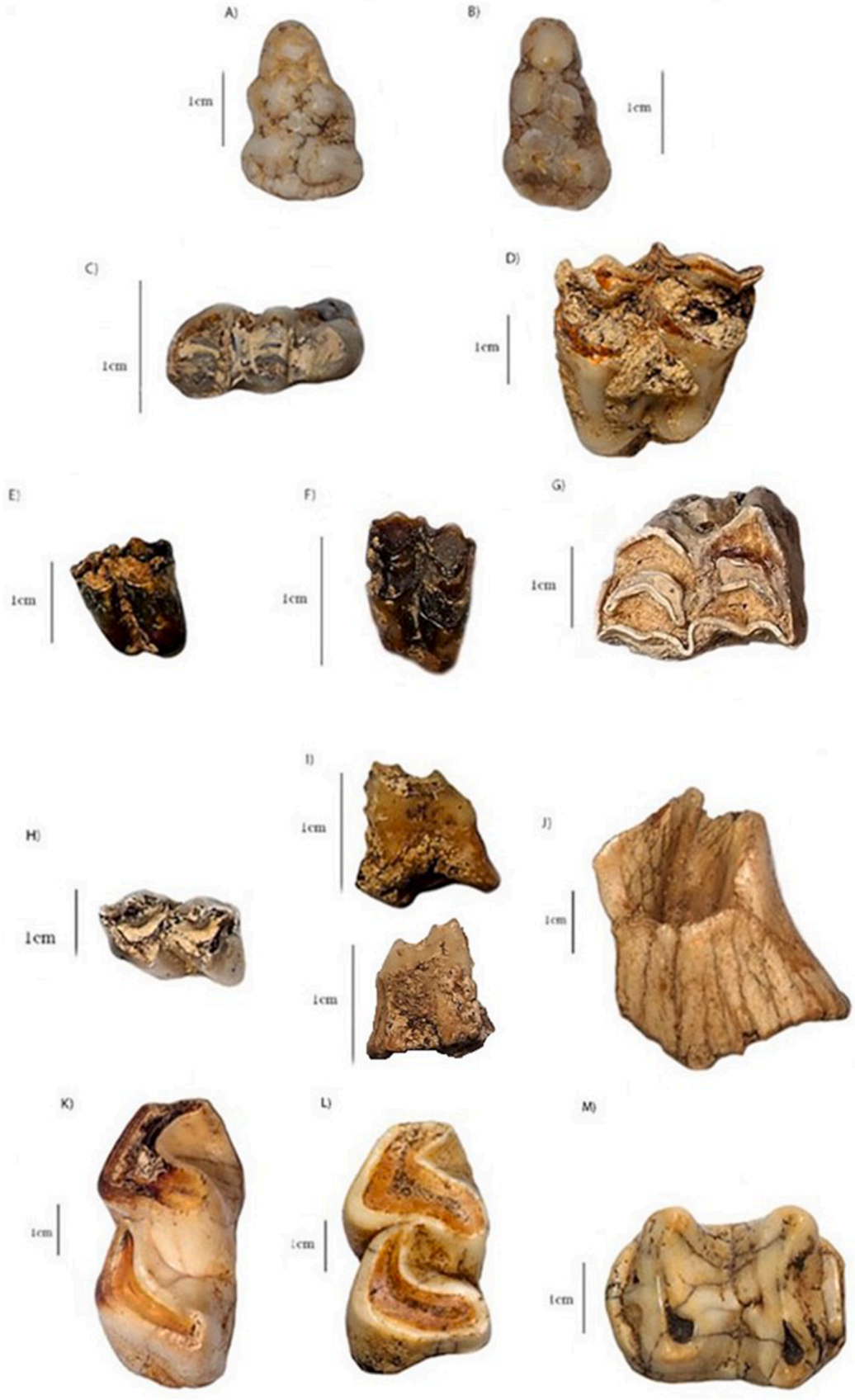

Fig. 7. (A) NG30.10 *Sus scrofa*, right M^3; (B) NG30.12 *Sus barbatus,* right M^3; (C) GG3.120 Tragulidae, m_3; (D) GU1 *Rusa* sp., left M1 from ex-situ deposits; (E) NG37.22 Cervidae, right M1; (F) NG32.18 *Muntiacus* sp., right M; (G) NG37.15 Bovidae, left M^3; (H) NG32.16 *Capricornis sumatraensis,* left m_2; (I) NG21.27 Moschidae, right P^4; (J) NG23.10 *Rhinoceros unicornis,* left M^1 fragment; (K) NG24.11 *Rhinoceros sondaicus,* left m_2; (L) NG24.10 *Dicerorhinus sumatrensis,* right m_2; (M) NG22.10 Tapiridae, right m_3.

Fig. 8. (Left) GG4.1 *Hexaprotodon* molar fragment; (right) modern *Choeropsis liberiensis* m2 from American Natural History Museum 81899 collection for comparison.

(See Fig. 8)

Hexaprotodon has been identified using variations in cranial and skeletal features between recent and fossil species and considered to be a peculiar lineage of hippopotamids in Asia (Falconer and Cautley, 1836; Lydekker, 1884; Colbert, 1935; Hooijer, 1950; Coryndon, 1970, 1977; Boisserie and White, 2004). Specimen GG4.1 consists of the anterior portion of a left m_2, which preserves the protoconid, metaconid, and a well-developed anterior cingulid. It is well worn with the cusp apices absent, and significant dentine exposed. It is most comparable to specimen 81899 of *Choeropsis liberiensis* from the American Museum of Natural History, which are similarly worn (Fig. 4). Specimen GG4.1 is slightly larger than AMNH81899, with a more anteriorly orientated metaconid, a wider and more prominently defined anterior cingulid that forms a wider and more deeply developed anterolingual basin between the anterior margin of the protoconid and the posterior lobe of the anterior cingulum.

Family: Tragulidae Milne-Edwards, 1864
Representative Specimen: GG3.120 – right m3 – NG-A assemblage

(Fig. 7C)

This specimen is identifiable as there are four sickle-shaped cusps on the crown of the molar show a characteristic bunoselenodont morphology (Rössner, 2007). Moreover, this tooth can now be identified as a lower molar of a Tragulidae due to the characteristic well-developed ectostylid and by far the largest cusp is the hypoconid, which projects rostrally (Farooq, 2008). This specimen cannot be identified to genus level as wear of the surface morphology has removed any evidence of the characteristic 'tragulus fold' in the basin of the pre-hypocristid.

Family: Cervidae Linnaeus, 1758
Genus: *Rusa* Kerr, 1792
Rusa sp.
Representative Specimen: GU1 – left M^1 – NG-B assemblage

(Fig. 7D)

This cervid tooth is much larger than the specimen described previously, with the maximum length of 23.94 mm and width of 24.67 mm taken at the base of the specimen crowns. These measurements compare best with that of *Rusa unicolor* but this taxonomic assignment cannot be confirmed. This tooth has a pronounced entostyle. The tooth has the typical features of a *Rusa* molar; a notably brachyodont crown composed of four main cusps with sharp lingual crests in two lophs (Leslie, 2011). The tooth is a first molar, evident as the accessory elements such as the mesial and distal cingulum and entostyle are notably weak, and the postcingulid and *Palaeomeryx*-fold are absent (Dong and Chen, 2015).

Genus: *Muntiacus* Martin, 1886
Muntiacus sp.
Representative Specimen: NG32.18 – right M – NG-B assemblage

(Fig. 7E)

NG32.18 is a square tooth with four crescentic cusps. The tooth has a rectolinear hypocone and rounded protocone. It displays a distinct and well-developed mesostyle that wedges into a more reduced, thinner parastyle. It displays a thick, crenulated cingulum. The fossa is obscured by matrix.

Cervidae gen et sp. indet.
Representative Specimen: NG37.22 –right M^1 – NG-B assemblage

(Fig. 7F)

NG37.22 is attributable to Cervidae due to the distinct selenodont morphology with broad cingulum and steeply sloped sides of the crowns (Hillson, 2016). It is a rectangular tooth and attributed as a first molar due to the more lingually protruding protocone relative to the hypocone. These morphological characteristics and the small size of the tooth suggest that this may be a Muntjak molar, though this cannot be confidently established.

Family: Bovidae Gray, 1821
Representative Specimen: NG37.15 – left M^3 – NG-B assemblage

(Fig. 7G)

The NG37.15 tooth attributed to a bovid is robust with pronounced and pointed styles, particularly the metastyle. The hypocone and protocone protrude lingually together but are split down the middle, producing a "W" shaped outline (Hillson, 2005). A developed metastylar wing in the tooth is similar to the specimens of *Naemorhedus sumatraensis* published in Tougard (1998) and Bacon et al. (2008), though this cannot be confirmed.

Genus: *Capricornis* Ogilby, 1836
Species: *Capricornis sumatraensis* Bechstein, 1799
Representative Specimen: NG32.16 – left m_2 - NG-B assemblage

(Fig. 7H)

The tooth is a hypsodont crown with smooth enamel, low depressed walls and a single infundibulum (Hooijer et al., 1958; Wattanapituksakul et al., 2018). The crown has narrow central fossa bounded by a ridged hypoconid and protoconid. The hypoconid is far more pronounced than that of the protoconid, and there is no evident ectostylid (Suraprasit et al., 2016).

Family: Moschidae Gray, 1821
Moschus Linnaeus, 1758
Moschus sp.
Representative Specimen: NG21.27 –right P^4 – NG-B assemblage

(Fig. 7I)

This specimen is moderately molariform, alike to modern P^4 representatives (Zhang et al., 2018). However, the talonid of the specimen is broad and approximately triangle, and the metacone is orientated distally; characteristic of a P^4. The tooth is selenodont with a well-developed but low crown, and high column-shaped flat lingual walls. The crown has a shallowly depressed central fossa enclosed by a prominent anterior metastyle and parastyle, and a posterior protocone. The anterior styles have much higher dimensions than the posterior of the crown.

Order: Perissodactyla Illiger, 1811
Family Rhinocerotidae Gray, 1820

Genus *Rhinoceros* Linnaeus, 1758
Rhinoceros unicornis Linnaeus, 1758
Representative Specimen: NG23.10 –left M^1 fragment - NG-B assemblage

(Fig. 7J)

The specimen is a posterior buccal fragment preserving the hypocone, partial metaloph, postfossette and posterior cingulum. A steep partial metaloph dips immediately into a deep, narrow concave postfossette, with the exterior lip of the postfossette descending broadly into a partial metaloph. The specimen has a V-shaped and considerably deep molar valley, which combined with its large size, suggests this tooth is attributable to *Rhinoceros unicornis* (Guérin, 1980; Laurie et al., 1983; Groves, 1983).

Rhinoceros sondaicus Desmarest, 1822
Representative Specimen: NG24.11 –left m_2 – NG-B assemblage

(Fig. 7K)

This second molar is identified as Rhinocerotidae as it displays the classic pair of U-shaped lophs (Tong and Guérin, 2009). It is distinguished from *Dicerorhinus* on the basis of relatively equal depths of the molar valleys (Groves, 1983; Tong and Guérin, 2009), and excluded from *Rhinoceros unicornis* on the basis of its smaller size (Guérin, 1980).

Genus: *Dicerorhinus* Gloger, 1841
Dicerorhinus sumatrensis Fischer, 1814
Representative Specimen: NG24.10 –right m_2 – NG-B assemblage

(Fig. 7L)

The tooth of Dicerorhinus sumatrensis is morphologically like that of Rhinoceros sondaicus. The features that distinguish the teeth of these species are subtle; the medial valley (trigonid pit) is much shallower than the distal valley (talonid pit) (Groves, 1983; Tong and Guérin, 2009).

Family: Tapiridae Gray, 1821
Genus: *Tapirus* Brünnich, 1772
Species: *Tapirus indicus* Desmarest, 1819
Representative Specimen: NG22.10 – right m_3 – NG-B assemblage

(Fig. 7M)

This molar of the Tapiridae is easily identifiable due to the characteristic brachydont low crowns with two distinct lophs separated by a long, straight traverse ridge (Hooijer, 1947b). The tooth is likely a third molar, evident as the talonid and trigonid are more or less equal, with a well-developed anterior cingulid. The dimensions of this specimen fall well within the morphology and size range for *Tapirus indicus* (Desmarest, 1819; Hooijer, 1947b; Tong, 2005; supplementary Table S7).

Order: Carnivora Bowdich, 1821
Family: Felidae Fischer de Waldheim, 1817
Subfamily: Felinae Fischer de Waldheim, 1817
Representative Specimen: NG15.17 – right m_1 – NG-B assemblage

(See Fig. 9, Fig. 9A)

The singular first molar is divided solely into two broad protoconid and paraconid blades. The protoconid diverge minimally towards the labial, and the paraconid diverges minimally towards the lingual, and these two conids converge at a short deep groove buccally. There is a shallow broad depression on the occlusal surface extending at a shallow angle from the tip of the conid blades. There is no evident metaconid or talonid on this tooth. This tooth morphology and size profile could plausibly fit the size profile of the three common feline species in Sumatra: the Asian Gold Cat (*Pardofelis temminckii*), the Marbled Cat (*Pardofelis marmorata*) and the Leopard Cat (*Prionailurus bengalensis*)

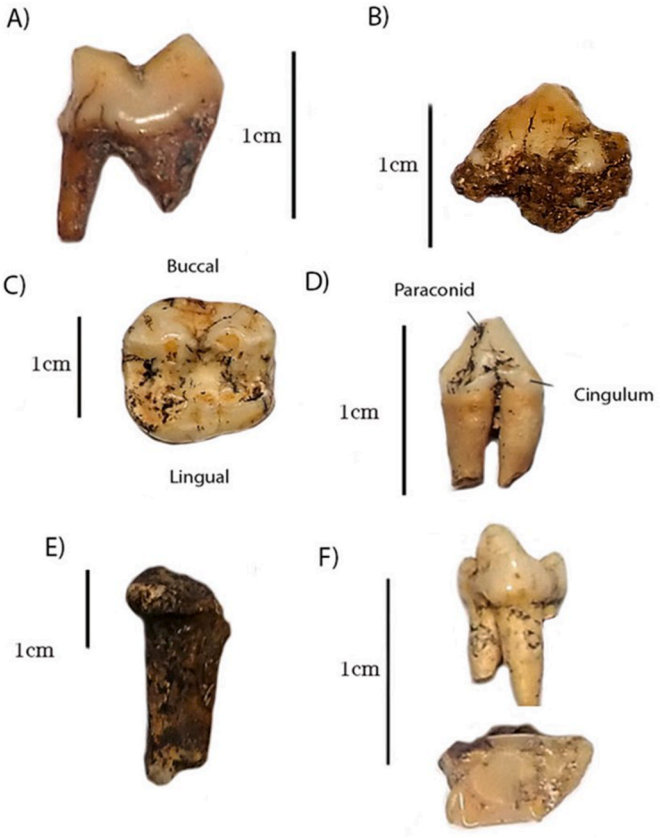

Fig. 9. (A) NG15.17 Felid, right m_1; (B) NG15.11 *Panthera tigris,* left p_3; (C) NG26.10 *Helarctos*, right M^1; (D) NG15.28 Mustelid, right p_4; (E) NG1.2 Viverridae, calcaneum; (F) (left) NG15.26 *Paradoxurus*, right m_1, disto-lingual view; (right) NG15.26 *Paradoxurus,* right m_1 occlusal view.

(Sunquist and Sunquist, 2009; Francis, 2017).

Genus: *Panthera* Oken, 1816
Representative Specimen: NG15.11 – left p_3 – NG-B assemblage

(Fig. 9B)

This specimen has the morphology of a third lower premolar (Hillson, 2005). There is a blunted protoconid with a main shearing crest, a small mesial paraconid and a small distal hypoconid that fit the morphology of a feline lower third premolar (Hooijer, 1947a). NG15.11 premolar conforms to the standard size variance best fits that of the *P. tigris* (Hooijer, 1947a; Badoux, 1959; Mazak, 1981; supplementary Table S8).

Family Ursidae Fischer de Waldheim, 1817
Genus *Helarctos* Raffles, 1821
Representative Specimen: NG26.10 – right M^1 – NG-B assemblage

(Fig. 9C)

This tooth is a broad, flat bunodont crown. It is nearly square in shape; a broad transverse valley separates the metacone and paracone from the lower protocone. The metacone and paracone are higher than that of the protocone. The mesial and distal edge of the metacone and paracone pinch into a small ridge. A deep notch separates the protocone and metacone. This molar conforms to those of the modern *Helarctos* (Raffles, 1821), and those excavated from similar cave sites in the region (Hooijer, 1948; de Vos, 1983; Long et al., 1996; Christiansen, 2008; supplementary Table S8).

Family: Mustelidae Fischer de Waldheim, 1817
Subfamily: Mustelinae Fischer de Waldheim, 1817

Representative Specimen: NG15.28 – right p_4 – NG-B assemblage

(Fig. 9D)

NG15.28 is a triangular monocuspid tooth with a sizeable pointed paraconid. This conid steeply slopes down to a stout shallow talonid basin surrounded by a prominent cingulum. These features are characteristic of a lower right fourth premolar of Mustelidae, though the dimensions overlap with numerous individuals and so cannot be determined to genus level (Popowics, 2003; Hillson, 2005; Peigné et al., 2009; Grohé et al., 2010).

Family: Viverridae Gray, 1821

Representative Specimen: NG1.2 – left calcaneum – NG-B assemblage

(Fig. 9E)

The specimen is a small calcaneum. The features distinctive of Viverridae are prominent and pointed sustentaculum tali at almost a right angle to the neck of the calcaneum and the process calcaneus is robust and square, with a distinct groove on the plantar surface (Stains, 1983).

Genus: *Paradoxurus* Cuvier 1822

c.f. *Paradoxurus* sp.

Representative Specimen: NG15.26 – right m_1 – NG-B assemblage

(Fig. 9F)

This bunodont tooth has a triangular outline in occlusal view. The buccal cusps are stout and rounded, with a reduced protoconid, large, bulbous paraconid, a well-developed, rounded metaconid, a bulbous cusp-like parastylid, with a small, poorly-developed metaconulid located in the valley between protoconid and paraconid. The paraconid is the highest cusp. The tooth lacks a distinct buccal cingulum. The tooth NG15.26 most resembles the modern palm civet (Gregory and Hellman, 1939; Popowics, 2003) and is tentatively identified as *Paradoxurus*.

4.2. U-series and ESR dating

4.2.1. ESR dose evaluation

The five samples measured by ESR are characterised by relatively weak ESR intensities, especially for the least irradiated aliquots, which is why acquisitions of up to 50 scans have been performed. However, many ESR spectra still show a non-horizontal baseline and low signal-to-noise ratio (<5), both of which may significantly bias the D_E evaluation. Consequently, a cubic baseline correction was employed for all ESR spectra as in Duval and Martín-Francés (2017), before extracting the T1-B2 ESR intensity. Additionally, the mean scan-normalized noise ESR intensity extracted from all the aliquots of a given sample measured at a given time was subtracted from the intensity of the radiation-induced ESR signals. Final D_E evaluation was performed using the baseline- and noise-corrected ESR intensities (Table S3 and Figure S1).

Measurement precision achieved is overall excellent, with all samples showing a variation of <2.5%. This results in a D_E repeatability that is systematically <5%, with the exception of SUM18-26 (6.4%). D_E values range between 20 and 40 Gy (Gy). Consequently, the dose-response curve of each sample was restricted to D_{max}/D_E ratios of between 5 and 10, in accordance with the recommendations of Duval and Grün (2016) (see Supplementary Information Table S3). This restriction on the maximum applied irradiation dose (D_{max}) has, however, only a very limited impact on the D_E estimates: they vary between −2% and +5% when considering the full dose range instead - but remain systematically within 1-σ consistent (Figure S1). No apparent D_E pattern is observed for the two loci: D_E estimates range from ~22 to ~35 Gy for NG-A teeth, while the two NG-B teeth provide very close results around 32–34 Gy.

4.2.2. Solution U-series analyses

4.2.2.1. Bulk analyses of dental tissues. U-series results associated with the ESR analyses are displayed in Table 1. 230Th/232Th ratios measured in all dental tissues are systematically >30, which indicates that contamination by detrital Th is minimal and has a very limited impact (<2%) on the apparent U-series ages. Enamel tissues show mostly very low uranium concentrations between 0.04 and 0.11 ppm; these samples yield apparent U-series ages ranging from between ca. 50 and 60 ka, except for sample SUM18-24, which displays a much older estimate of about 90 ka. Dentine tissues show higher concentration values that vary within a narrow range (3.37–5.28 ppm). The apparent U-series ages are systematically younger compared with the enamel layer from the same tooth, between 28.6 and 48.9 ka. This different age pattern between is reinforced by the initial 234U/238U ratio calculated for each sample: it varies between 1.071 and 1.110 for the dentine samples and 1.208–1.390 for the enamel, suggesting that enamel and dentine may have experienced different uranium uptake processes. The dentine being usually more sensitive than enamel to any geochemical/diagenetic changes in the surrounding environment, we suspect that dentine tissues may have been impacted by a more recent U uptake event. Without spatially resolved U-series data, it is, however, currently impossible to draw any further conclusion from the present data set.

Interestingly, the U-series data collected for fossil teeth from NG-A and NG-B show a slightly different pattern: enamel tissues from NG-B return the oldest U-series ages in comparison with those from NG-A (61–91 ka vs. 52–59 ka), and similar observations can be made for the dentine tissues (45–49 ka vs. 28–42 ka).

4.2.2.2. U concentration and age profiling for GG4.1. We also produced five independent U-series ages for the *Hexaprotodon* specimen GG4.1 (Table 2). Uranium concentration is lowest for the enamel (ca. 2 ppm) but also yielded the oldest 230Th age (ca. 85 ka). The dentine portions contained a higher concentration of uranium (ca. 7–13 ppm) and systematically lower ages of ca. 76–73 ka, like the other dated samples above. Similarly, there are high 230Th/232Th activity ratio suggesting that detrital contaminants do not substantially affect the uncorrected versus corrected ages.

GG4.1 differ from the other dated teeth in many aspects. For example, the apparent U-series ages in the dentine are systematically younger than those measured in the other teeth (Table 1). Similarly, measured and initial 234U/238U activity ratios are lower, which may suggest a different uptake history and/or geochemical environment for this specimen. The tooth is not ideal for U-series dating given the variability in uranium concentration through the tooth, especially the dentine. This variability might also partly explain the reason for such distinct U-series data among the teeth. However, several ages of GG4.1 dentine are clustered around 68–72 ka. There may be multiple phases of U-uptake in the tooth, but there is no clear evidence of U-leaching. We are confident that the tooth has produced reliable minimum ages of around 56–73 ka. Significantly this age interpretation is consistent with other teeth dated with the combined U-series/ESR approach detailed below.

4.2.3. Combined U-series and ESR age calculations

Among all the initial ESR age calculations (samples labelled “a” in Table 1), only one sample (SUM18-21a) returned a finite combined US-ESR age result (134 + 12–11 ka). A very close CSUS-ESR estimate of 141 ± 13 ka was obtained for this tooth, which indicates that the modelling of uranium uptake into dental tissues has a negligible impact on the calculated age. This is due to the limited contribution of dental tissues to the total dose rate (about 13%).

Initial combined US-ESR age calculations did not return results for the other samples (SUM18-22a, SUM18-24a, SUM18-26a, SUM18-27a), suggesting thus that dental tissues may have experienced uranium